Experimental and model based investigation of the links between snow bidirectional reflectance and snow microstructure

M. Dumont[1], F. Flin[1], A. Malinka[2], O. Brissaud[3], P. Lapalus[1], P. Hagenmuller[1], B. Lesaffre[1], A. Dufour[1], N . Calonne[1,4], S. Rolland du Roscoat[5] and E. Ando[5]

[1] Météo-France - CNRS, CNRM UMR 3589, Centre d'Etudes de la Neige (CEN), Grenoble, France ; [2] Institute of Physics, National Academy of Sciences of Belarus, Minsk, Belarus ; [3] Univ. Grenoble Alpes - CNRS, IPAG, Grenoble, France
[4] Montana State University, Bozeman, USA ; [5] UGA - Grenoble INP - CNRS, 3SR UMR 5521, Grenoble, France

Contact: marie.dumont@meteo.fr

Overview

This work presents measurements of snow bi-directional reflectance (BRDF) in cold room along with micro-computed tomography (CT) of the snow. Measurements are compared to simulations of reflectance obtained with the model of *Malinka*, *2014*. We investigate the effects of snow microstructure treatment and uncertainties on the value of the ice refractive index on the simulations.

Measurements

BRDF set-up

Figure 1 – S1 in the spectro-goniradiometer. Illumination in the right arm, the left arm is reflected light measurements.

FOV 2.05° → the difference between the measurements and BRDF values is negligible (*Nicodemus et al., 1977*)

Tomography

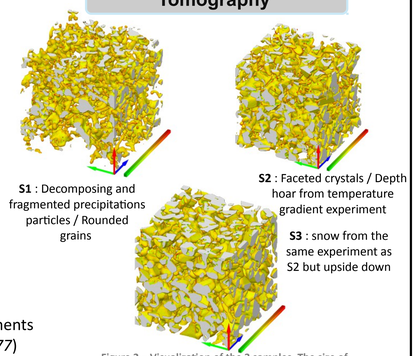

Figure 2 – Visualization of the 3 samples. The size of the cube is approximately 7 mm. The color is proportional to the curvature

Table 2. Geometry and spectral range of S1 optical measurements

Name	θ_i	ϕ_{view}	θ_{view}	spectral range	begin	end
2012_run1	30	180	70,60,50,45,40,30,20,10,0	1500,1520 nm	03-27 15:23	03-27 15:31
2012_run2a	30	0,30,60,90,120,150,180	0,15,30,45,60,70	700-1540 nm step 20 nm	03-27 15:59	03-28 00:20
2012_run3a	60	180	70,65,60,50,40,30,20,10,0	1280-2500 nm step 20 nm	03-28 08:48	03-28 11:55
2012_run4a	0	0,90,180	15,20,30,35,40,45,50, 55,60,65,70	800, 810 nm	03-28 14:14	03-28 14:39
2012_run5a	0	0,90,180	15,20,30,35,40,45,50, 55,60,65,70	1300, 1310 nm	03-28 15:13	03-28 15:38
2012_run6a	0	0,90,180	15,20,30,35,40,45,50, 55,60,65,70	900-1090 nm step 10 nm	03-28 16:10	03-28 19:43
2012_run7a	30	180	70,60,50,45,40,30,20,10,0	1500, 1520 nm	03-29 08:17	03-29 08:24

Reflectance processing

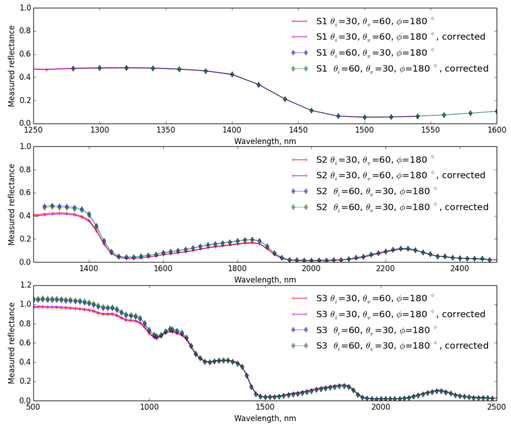

Figure 3 – Comparison of reflectance obtained for optically equivalent geometries for the 3 samples. Corrected means corrected for not perfectly horizontal surface.

References scans at the beginning and at the end of the experiments show that the reflectance slightly evolves during the experiment (small changes in SSA and sublimation)

Planeity correction was performed using the differences in reflectances obtained for nadir illumination at several azimuths (small slope angles -0.24°, -0.59° and -0.52° were estimated).

The reciprocity principle is not completely verified (see Fig. 3 on the left) due to :

- Changes in snow during the scan.
- Re-illumination effects at high incident zenith angle (60°).

CT image analyses

3D images were first segmented and then analyzed. Several properties, including SSA and density were estimated from the images using two methods : (i) the voxel projection method described in *Flin et al. (2011)* (VP) and (ii) from the chord length distributions (CLD) using equation (5) in *Malinka (2014).*

Figure 4 shows that:

- The agreement between SSA estimated from CLD and from *Flin et al. (2011)* is good but there is a small positive bias between the two for low SSA and negative bias for higher SSA (r^2=0.994).
- The SSA estimated from DUFISSS measurements are systematically higher than the one estimated from 3D images.
- The SSA of the samples evolves slightly during the BRDF measurements for S1 and S3. For S2, the evolution is stronger.

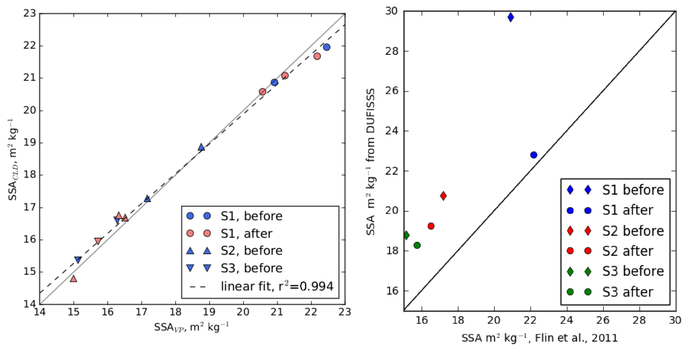

Figure 4 – Left panel: SSA obtained from chord length distributions versus obtained with the VP method (*Flin et al , 2011*) on the 3D images. Right panel: SSA measured using DUFISSS at 1310 nm (*Gallet et al., 2009*) versus SSA calculated using the VP method from *Flin et al. (2011).*

BRDF modeling

Reflectance modeling was performed using *Malinka's (2014)* model. This model is based on considering the snow as a two-phase random mixture of ice and air. The model uses geometrical optics laws and the steorological approach to compute inherent optical properties of snow based on the ice refractive index and on the CLD in ice and air.
The model was successfully evaluated in *Malinka et al. (2016)* and used in *Krol and Löwe (2016)* to relate optical properties to snow microstructure metrics.

In this work, two configurations for simulations are used:
- simulations using exponential CLD and SSA values estimated from the 3D images (herafter labelled 'exp')
- simulations using directly the CLD computed from the 3D images (herafter labelled 'CLD')

For both simulations, the amount of light absorbing impurities was estimated using a fit between the model and the measurements in the visible range.

Spectral reflectances

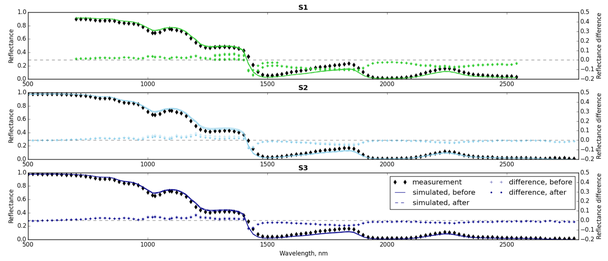

Figure 5 – Measured and simulated reflectances for the 3 samples. The incident zenith angles is 30°.
The viewing zenith angle is 60° and the measurements is taken in the principal plane (forward direction).

Carmagnola, C.M., Domine, F., Dumont, M., Wright, P., Strellis, B., Bergin, M., Dibb, J., Picard, G., Libois, Q., Arnaud, L. and Morin, S., 2013. Snow spectral albedo at Summit, Greenland: measurements and numerical simulations based on physical and chemical properties of the snowpack. *The Cryosphere*, 7(4), pp.1139-1160.
Flin, F., Lesaffre, B., Dufour, A., Gillibert, L., Hasan, A., Rolland du Roscoat, S., Cabanes, S. and Pugliese, P., 2011. On the computations of specific surface area and specific grain contact area from snow 3D images. *Physics and Chemistry of Ice*, pp.321-328.
Malinka, A.V., 2014. Light scattering in porous materials: Geometrical optics and stereological approach. *Journal of Quantitative Spectroscopy and Radiative Transfer*, 141, pp.14-23.
Malinka, A., Zege, E., Heygster, G. and Istomina, L., 2016. Reflective properties of white sea ice and snow. *The Cryosphere*, 10(6), p.2541.
Nicodemus, F.E., et al. 1977. Geometrical considerations and nomenclature for reflectance (Vol. 160). US Department of Commerce, National Bureau of Standards.
Krol, Q. and Löwe, H., 2016. Relating optical and microwave grain metrics of snow: the relevance of grain shape. *The Cryosphere*, 10(6), pp.2847-2863.
Grundy, W.M. and Schmitt, B., 1998. The temperature-dependent near-infrared absorption spectrum of hexagonal ice. *J. Geophys. Res*, 103, pp.25809-25822.
Warren, S.G., 1984. Optical constants of ice from the ultraviolet to the microwave. *Applied optics*, 23(8), pp.1206-1225.
Warren, S.G. and Brandt, R.E., 2008. Optical constants of ice from the ultraviolet to the microwave: A revised compilation. *Journal of Geophysical Research: Atmospheres*, 113(D14).

Results and future work

The simulated reflectances are in good agreement with the measured reflectances. Discrepancies are found in the NIR regions and can be partly attributed to the values of the ice refractive index as already noticed in previous work (*Carmagnola et al., 2013*).

Accounting for CLD estimations only impacts reflectances values for absorbing wavelengths and in the forward scattering angles as theoretically shown in *Krol and Löwe, 2016*. The effect of the refractive index uncertainty, especially of its imaginary part, is much more pronounced that the impact of other factors, such as the exact shape of the CLD, the anisotropy in the grain facet orientation, or the vertical heterogeneity of the sample.

Angular distribution

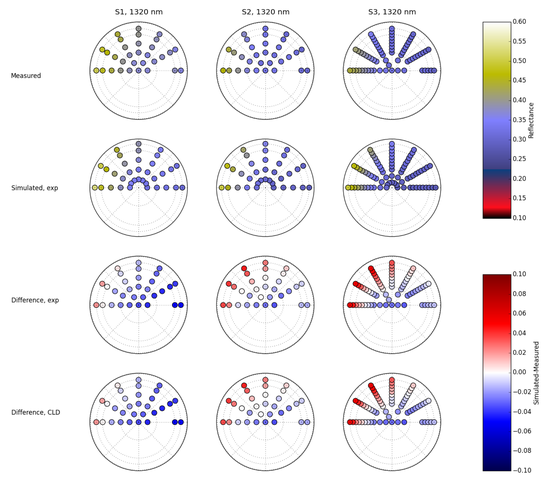

Figure 6 – Measured and simulated BRDF for the 3 samples. The incident zenith angles is 30°. In the polar plot, the radius is proportional to the viewing zenith angle and the azimuth is the relative azimuth between the viewing and incident azimuth. The data are for 1320 nm. Simulated data correspond to exponential CLD. Differences between the measured values and the two simulations are reported on the two last lines.

Forward scattering for absorbing wavelengths

Figure 7 – Measured (crosses) and simulated (dotted and plain lines) value of parameter η obtained for the 3 samples. EXP simulations correspond to plain lines and CLD to dotted lines.

$$\eta(\lambda) = \frac{R(30°,70°,180°,\lambda) - R(30°,70°,0°,\lambda)}{R(30°,70°,180°,\lambda)}$$

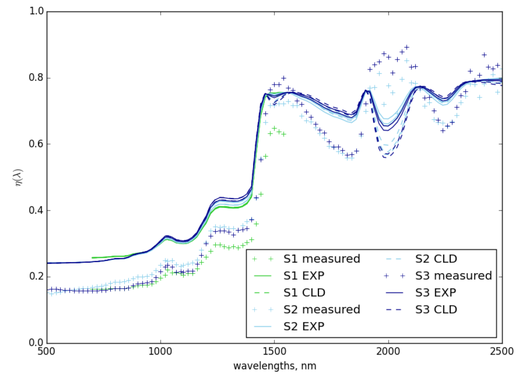

ACKNOWLEDGEMENTS

CEN and IPAG are part of Labex OSUG@2020. The authors are also grateful to Ghislain Picard, Quentin Libois, Quirine Krol and Henning Löwe for useful discussions on this study.

CNRM UMR 3589